Science Advances
AAAS

advances.sciencemag.org/cgi/content/full/6/13/eaaz3152/DC1

Supplementary Materials for

The insulator functions of the *Drosophila* polydactyl C2H2 zinc finger protein CTCF: Necessity versus sufficiency

Olga Kyrchanova*, Oksana Maksimenko, Airat Ibragimov, Vladimir Sokolov, Nikolay Postika, Maria Lukyanova, Paul Schedl, Pavel Georgiev*

*Corresponding author. Email: olgina73@gmail.com (O.K.); georgiev_p@mail.ru (P.G.)

Published 25 March 2020, *Sci. Adv.* **6**, eaaz3152 (2020)
DOI: 10.1126/sciadv.aaz3152

This PDF file includes:

Supplementary Methods
Fig. S1. Morphology of the abdominal segments (numbered) in males carrying different variants of the *Fab-8* or CTCF site replacements in Fab-7^{attP50} in the dark field.
Fig. S2. Morphology of the abdominal segments (numbered) in males carrying different variants of *Mcp* in *Fab-*7^{attP50} in the dark field.
Fig. S3. Morphology of the abdominal segments (numbered) in males carrying different variants of $F2^{177}$ in *Fab-*7^{attP50} in the dark field.
Fig. S4. In vitro binding of dCTCF and Su(Hw) to $F2^{177}$and its derivatives.
Fig. S5. Strategy for creating *Fub* replacement lines.
Fig. S6. A lateral view of abd-A expression patterns in stage 14 embryos carrying different substitutions in $F2^{attP}$.
Fig. S7. *Ubx* expression in $F2^{attP}$, *F2177*, and *F2177DC*, exhibiting wing phenotypes.

Supplementary Methods

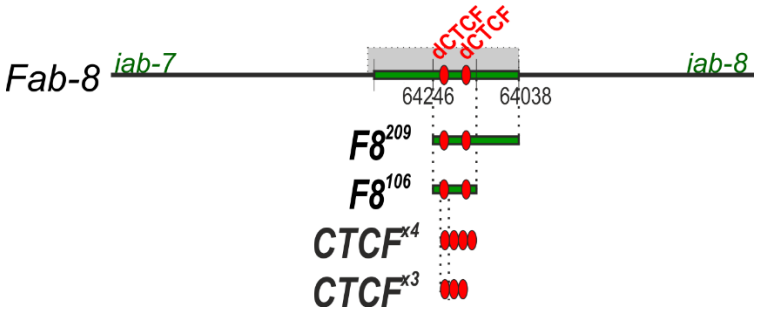

CTCF bs

F8^{209}

actttaaatttccacattcccgccttGCAGCGCCACCTGGCCTTGGtaatgtagaactaggaaggaaagcac
caaCACAAGATGTCGCTCTCCGACagtggacatgtcgcgtaaaaaatgttcgataactttcaatggttcgatt
gaacagacaataagtgtatttaagacaccagttcttatattcaaaaatcctaacaactcacatt

F8^{106}

actttaaatttccacattcccgccttGCAGCGCCACCTGGCCTTGGtaatgtagaactaggaaggaaagcac
caaCACAAGATGTCGCTCTCCGACagtggacatg

CTCF^{x4}

*actagt*gctGCAGCGCCACCTGGCCTTGGagatcctGCAGCGCCACCTGGCCTTGGagatc
ctGCAGCGCCACCTGGCCTTGGagatctCCAAGGCCAGGTGGCGCTGCAgc*cccggg*

CTCF^{x3}

*actagt*gctGCAGCGCCACCTGGCCTTGGagatcctGCAGCGCCACCTGGCCTTGGagatc
ctGCAGCGCCACCTGGCCTTGG*agatct*

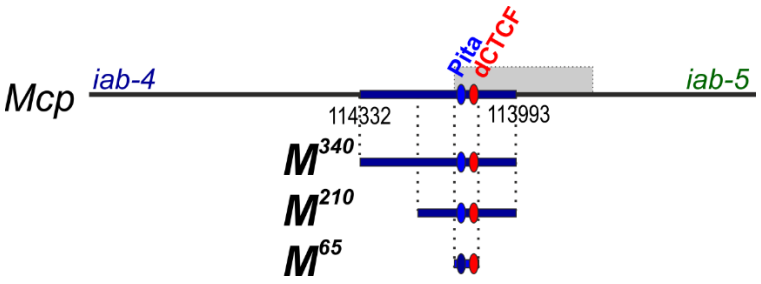

Pita bs; CTCF bs

M^{340}

gctcagagtacataagcgacgcccaaaaagcccaaatgtagagctttttcgaaattaaacagaaagtcgggtctgcaaa
taagggcttttctggggaagaaataaattatatcttaataaatatattttaaacttaactcagacttggatttattttgaactacac
acttaagtgatttaaataatttttaaatatatttcttacataaattTAGCCAATATCCAAACCTttttgcgctGGCGC
CCCCTATTGTTTTTCtttcgcagctcatgctttgctggcaacccaccagaggacgctcgctgattgaatcgcattac
gcacacttacaacgattggg

M^{210}

aacttaactcagacttggatttattttgaactacacacttaagtgatttaaataatttttaaatatatttcttacataaattTAGCC
AATATCCAAACCTttttgcgctGGCGCCCCCTATTGTTTTTCtttcgcagctcatgctttgctggcaacc
caccagaggacgctcgctgattgaatcgcattacgcacacttacaacgattggg

M^{210}

aattTAGCCAATATCCAAACCTtttgcgctGGCGCCCCCTATTGTTTTTCttttgcagcttatgc

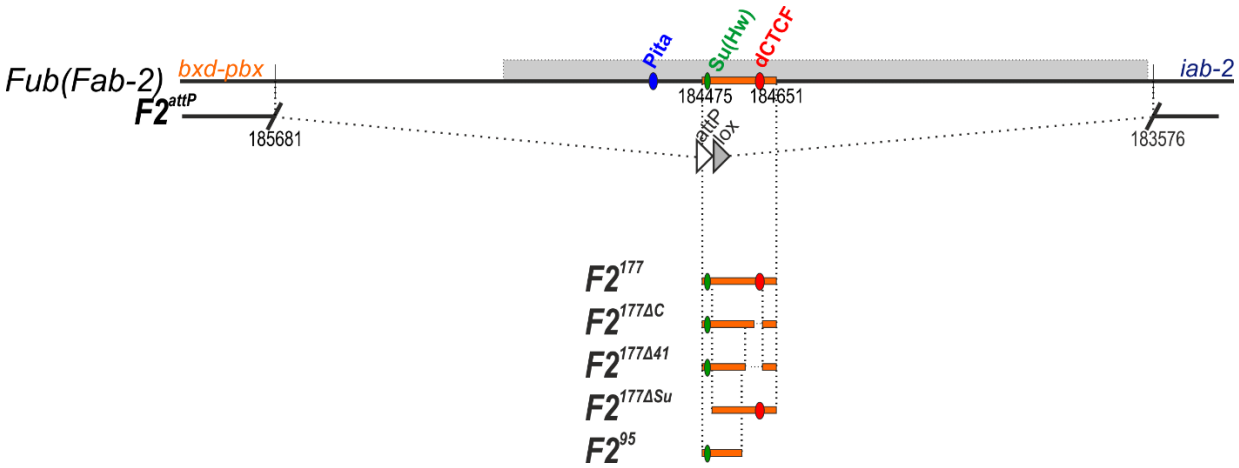

Su(Hw) bs; CTCF bs

F2^{177}

atgcctAAAAGTATGCAGAAatttgttcaacaagtctgcttatgtgcaccctctcgcgatcggtggcataaccaatcg
aggattcagctcttgagctacctGCCGAAAGGGGCGCGGCgaccttaagGGCGACATCTATATCT
CGCATagtgtgcagaactgcttgttcctagtcac

F2$^{177\Delta C}$

atgcctAAAAGTATGCAGAAatttgttcaacaagtctgcttatgtgcaccctctcgcgatcggtggcataaccaatcg
aggattcagctcttgagctacctgccgaaaggggcgcggcaacctt***aagctt***GCATagtgtgcagaactgcttgttccta
gtcac

F2$^{177\Delta Su}$

gttcaacaagtctgcttatgtgcaccctctcgcgatcggtggcataaccaatcgaggattcagctcttgagctacctGCCG
AAAGGGGCGCGGCgaccttaagGGCGACATCTATATCTCGCATagtgtgcagaactgcttgttcct
agtcac

F2$^{177\Delta 41}$

atgcctAAAAGTATGCAGAAatttgttcaacaagtctgcttatgtgcaccctctcgcgatcggtggcataaccaatcg
aggattcagctcttgagctacctgc***aagctt***GCATagtgtgcagaactgcttgttcctagtcac

F2$^{177\Delta 21}$

atgcctAAAAGTATGCAGAAatttgttcaacaagtctgcttatgtgcaccctctcgcgatcggtggcataaccaatcg
aggattcagctcttgagctacctgc***aagctt***aagGGCGACATCTATATCTCGCATagtgtgcagaactgctt
gttcctagtcac

F2^{95}

atgcctAAAAGTATGCAGAAatttgttcaacaagtctgcttatgtgcaccctctcgcgatcggtggcataaccaatcg
aggattcagctcttgag

Supplementary Figures

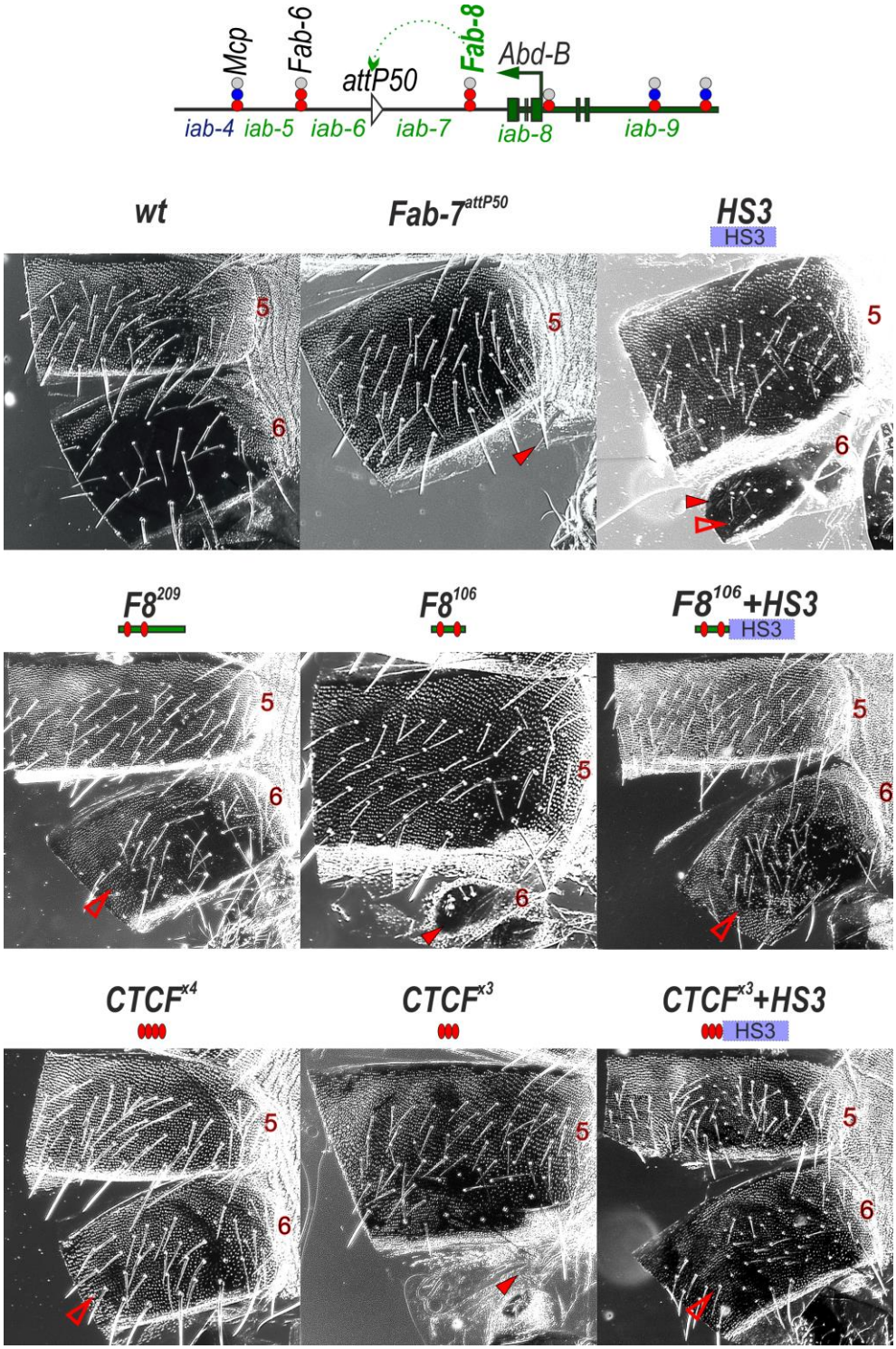

Fig. S1. Morphology of the abdominal segments (numbered) in males carrying different variants of the *Fab-8* or CTCF site replacements in Fab-7^{attP50} in the dark field. dCTCF and Pita binding sites at the boundaries are shown as red and blue circles/ovals respectively. The filled red arrows show the signs of the GOF phenotype (transformation of the A6 segment into A7). The empty red arrows show the signs of the LOF transformation (transformation of the A6 segment into A5). In wild-type males, trichomes cover the surface of the A5 tergite and only a thin stripe along the anterior and ventral edges of the A6 tergite. In $F8^{209}$, $F8^{106}$+*HS3*, $CTCF^{x4}$, and $CTCF^{x3}$+*HS3* males, the A5 and A6 tergites are completely covered with trichomes, supporting A6→A5 transformation.

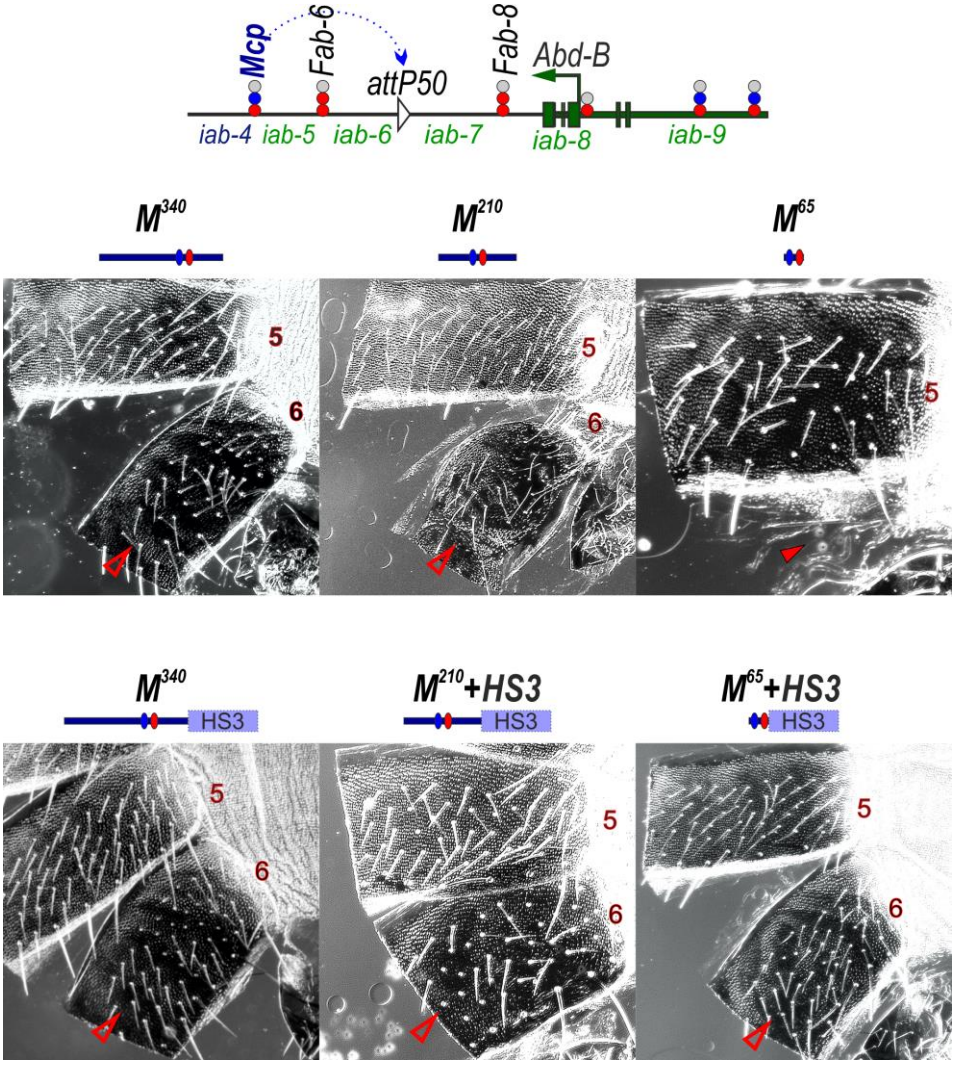

Fig. S2. Morphology of the abdominal segments (numbered) in males carrying different variants of *Mcp* in *Fab-7*^{attP50} in the dark field. The designations are the same as those in fig. S1.

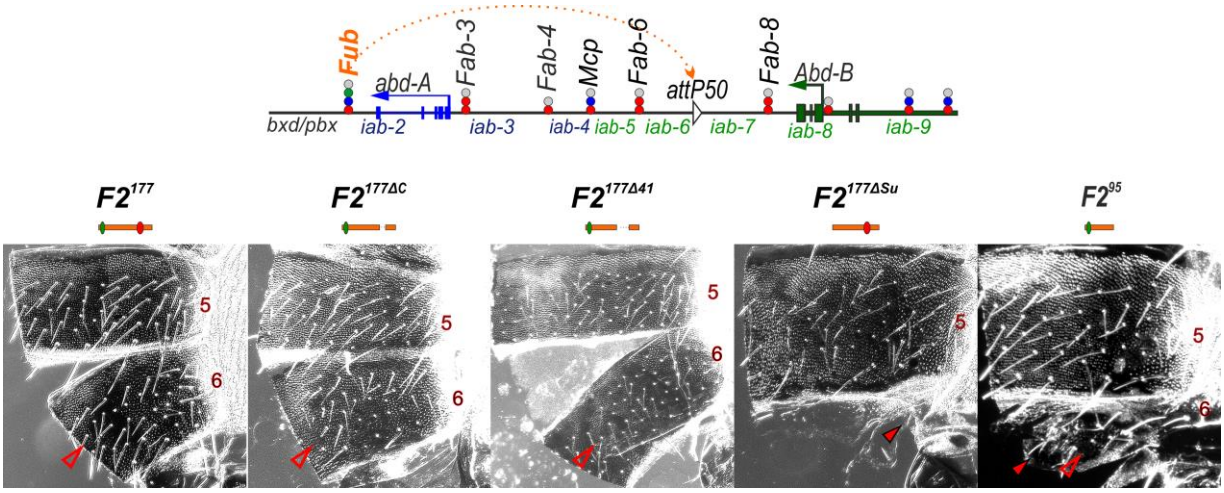

Fig. S3. Morphology of the abdominal segments (numbered) in males carrying different variants of *F2*^{177} in *Fab-7*^{attP50} in the dark field. The Su(Hw) binding site at the Fub boundary is shown as green circle/oval. The designations are the same as those in fig. S1.

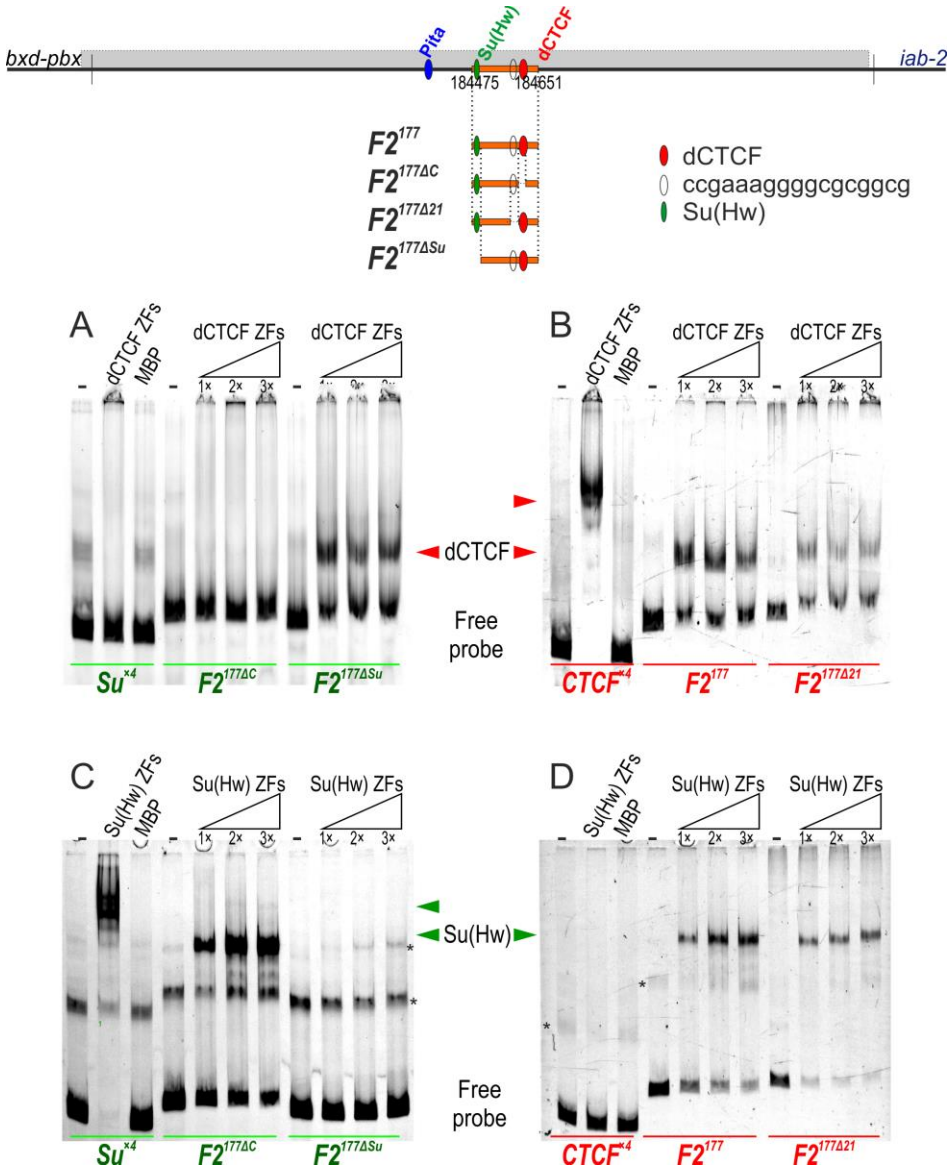

Fig. S4. In vitro binding of dCTCF and Su(Hw) to *F2*^{177} and its derivatives. For electrophoretic mobility shift assays, the zinc finger (ZF) clusters of dCTCF (11 ZF domains) and Su(Hw) (12 ZF domains) fused with Maltose-binding protein (MBP) were expressed in bacteria. MBP alone was used as the negative control. Fluorescently labeled DNA fragments (FAM or Cy5) were incubated with different amounts of proteins. Signals were detected at an excitation of 500 nm and an emission of 535 nm for FAM-labeled fragments and at an excitation of 630 nm and an emission of 700 nm for Cy5-labeled fragments. **(A)** FAM-labeled fragments (green). Only *F2*$^{177\Delta Su}$ demonstrated a strong and specific interaction with dCTCF ZFs, in contrast with *F2*$^{177\Delta C}$ or four Su(Hw) binding sites (Su$^{\times 4}$, used as a negative control for binding), which did not interact with dCTCF. **(B)** Cy5-labeled fragments (red). dCTCF ZFs effectively binds to four dCTCF binding sites (CFCF$^{\times 4}$, used as a positive control for binding), *F2*^{177} and *F2*$^{177\Delta 21}$. **(C)** FAM-labeled fragments (green). *F2*$^{177\Delta C}$ demonstrates a strong and specific interaction with Su(Hw) ZFs, similar to Su$^{\times 4}$. In *F2*$^{177\Delta Su}$, the deletion of the Su(Hw) binding site leads to the abolishment of Su(Hw) binding. * designates non-specific bands that are visible in negative samples. **(D)** Cy5-labeled fragments (red). Su(Hw) ZFs cannot bind to CFCF$^{\times 4}$ (used as a negative control for binding) but effectively bind to *F2*^{177} and with *F2*$^{177\Delta 21}$.

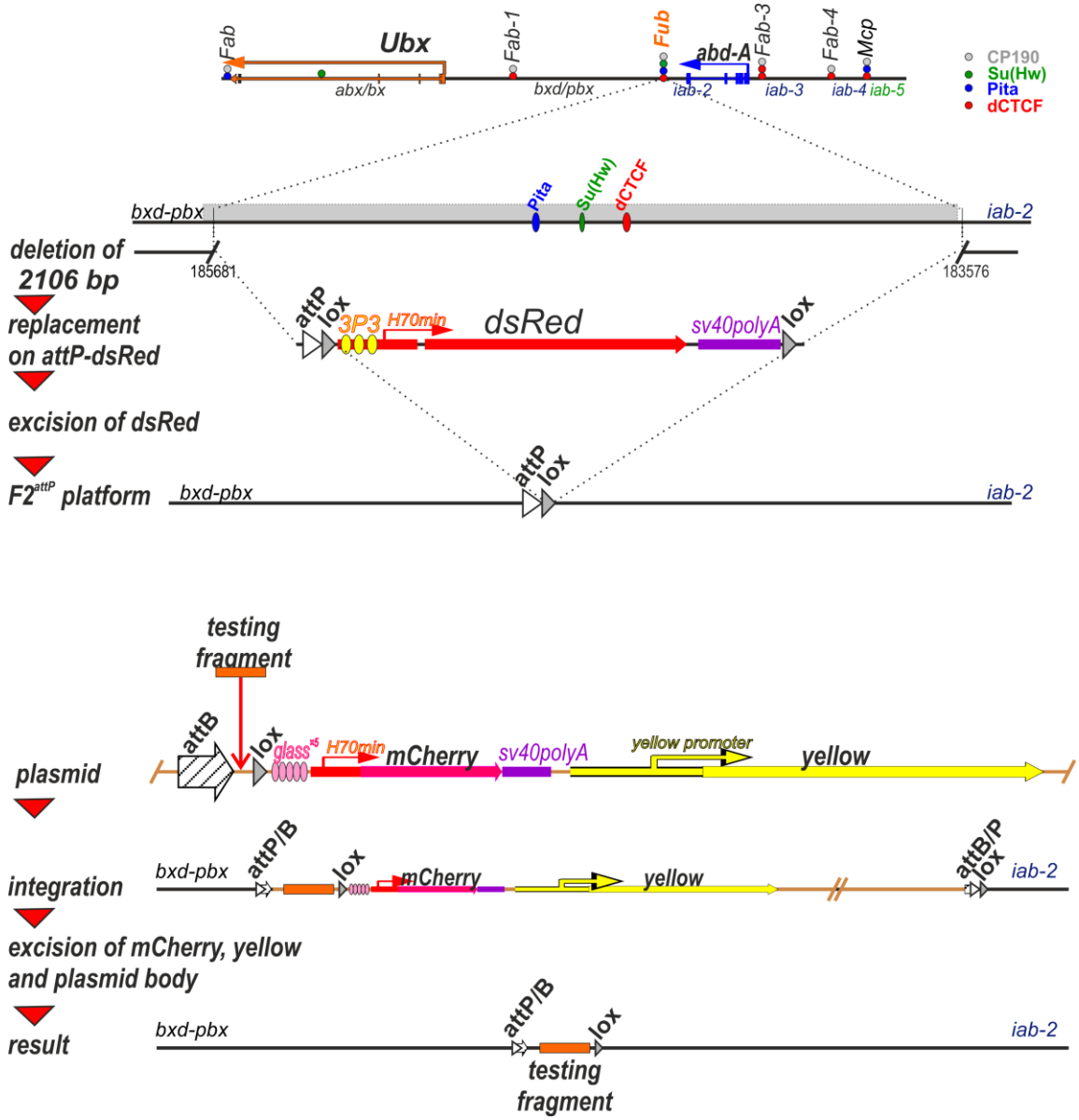

Fig. S5. Strategy for creating *Fub* replacement lines. Top: schematic representation of the regulatory region containing the *Ubx* and *abd-A* genes. The coding regions of the *Ubx* and *abd-A* genes are indicated by orange and blue arrows, respectively. The $F2^{attP}$ line was obtained through the substitution of a 2106-bp region with *attP* site and the *dsRed* gene, flanked by *lox* sites. The coordinates of the deletion, based on the complete sequence of BX-C (using SEQ89E numbering) are 185681–183576. During the final step, the *dsRed* gene was deleted by recombination between the *lox* sites. The plasmid that was injected into the $F2^{attP}$ line contains the *attB* site for integration and the *lox* site for the excision of the *yellow* and *mCherry* reporters. Both reporters, *yellow* and *mCherry*, were excised by Cre-mediated recombination between the *lox* sites. As a result, the testing elements were inserted in place of the 2106-bp deletion.

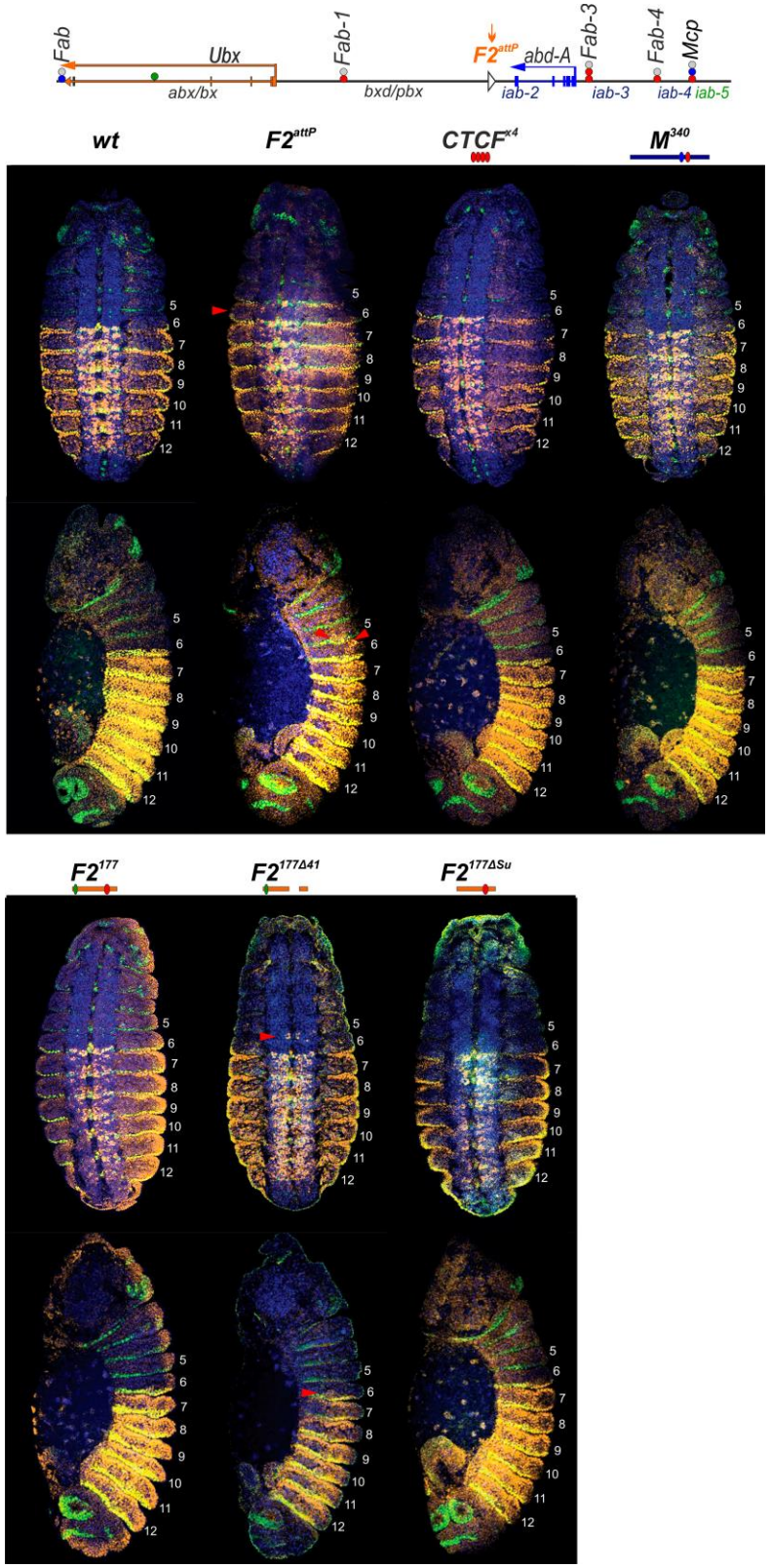

Fig. S6. A lateral view of abd-A expression patterns in stage 14 embryos carrying different substitutions in *F2^{attP}*. Each panel shows a confocal image of an embryo, stained with Abd-A (yellow) and Engrailed (En, green). DAPI was used to stain nuclei (blue). En is used to mark the parasegments, which are numbered from 5 to 12, on the right side each embryo image. Red arrows indicate the ectopic expression of Abd-A.

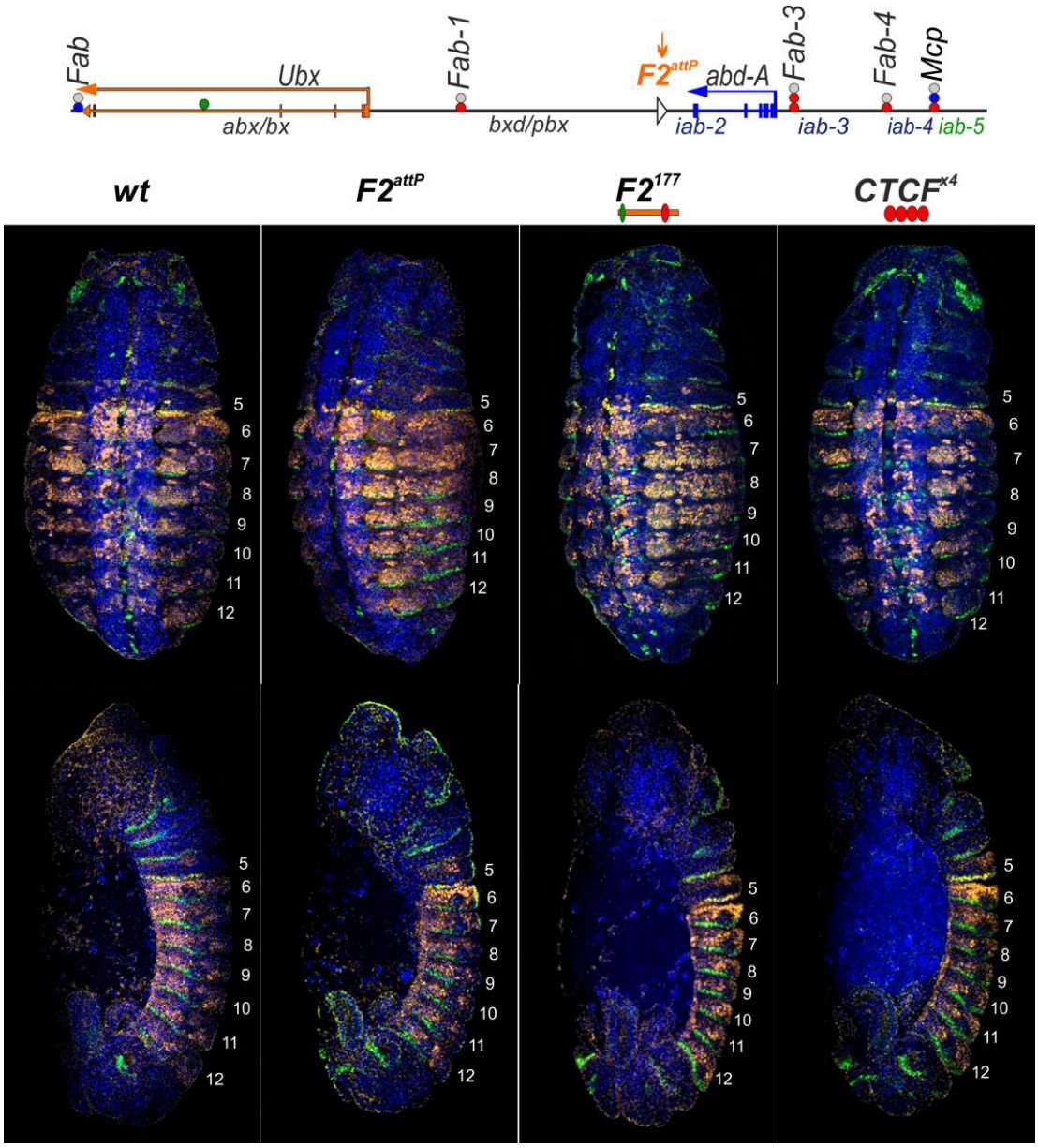

Fig. S7. *Ubx* expression in *F2^{attP}*, *F2177*, and *F2177DC*, exhibiting wing phenotypes. Lateral view in the top row, ventral view of the corresponding strain in the bottom row. Embryos at stage 14 were immunostained for *Ubx* (yellow) and engrailed (en, green) proteins, DAPI was used to stain the nuclei (blue). *Ubx* expression patterns in all three mutant strains resemble that in the wild-type (*wt*).